THE JOURNAL OF PHYSICAL CHEMISTRY LETTERS
A JOURNAL OF THE AMERICAN CHEMICAL SOCIETY

pubs.acs.org/JPCL

Letter

Ultrafast Internal Conversion Dynamics through the on-the-Fly Simulation of Transient Absorption Pump−Probe Spectra with Different Electronic Structure Methods

Chao Xu, Kunni Lin, Deping Hu, Feng Long Gu, Maxim F. Gelin, and Zhenggang Lan*

Cite This: *J. Phys. Chem. Lett.* 2022, 13, 661−668

Read Online

ACCESS | Metrics & More | Article Recommendations | Supporting Information

ABSTRACT: An on-the-fly surface-hopping simulation protocol is developed for the evaluation of transient absorption (TA) pump−probe (PP) signals of molecular systems exhibiting internal conversion to the electronic ground state. We study the nonadiabatic dynamics of azomethane and the associating TA PP spectra at three levels of the electronic-structure theory, OM2/MRCI, SA-CASSCF, and XMS-CASPT2. The impact of these methods on the population dynamics and time-resolved TA PP signals is substantially different. This difference is attributed to the strong non-Condon effects that must be taken into account for the proper understanding and interpretation of time-resolved TA PP signals of nonadiabatic polyatomic systems. This shows that the combination of the dynamical and spectral simulations definitely provides more accurate and detailed information on the microscopic mechanisms of photophysical and photochemical processes. Hence the simulation of time-resolved spectroscopic signals provides another important dimension to examine the accuracy of quantum chemistry methods.

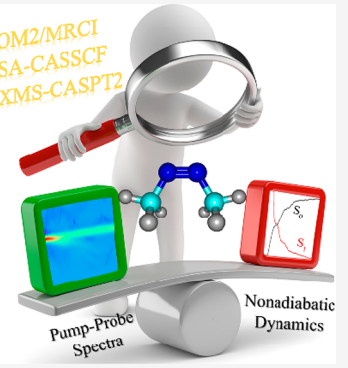

Light-driven nonadiabatic processes are essential in many photophysical, photochemical, and photobiological reactions.[1−6] A comprehensive understanding of these processes is fundamentally significant for uncovering the microscopic mechanisms of photoswitching,[7,8] photosynthesis,[9,10] and photostability.[11,12]

Time-resolved optical spectroscopy is a powerful experimental technique to study photoinduced nonadiabatic dynamics.[5,11−14] However, it is not straightforward to associate the directly measured spectroscopic observables with specific photochemical or photophysical processes without the preknowledge of excited-state dynamics therein. Therefore, the interpretation of spectroscopic signals relies heavily on the support from theoretical calculations and simulations.[14−20] The theoretical explanation of most time-resolved nonlinear spectroscopic signals is based on the third-order nonlinear optical response of the light-matter interaction.[21−23] In commonly used transient absorption (TA) pump−probe (PP) experiments, the system is perturbed by a pump laser pulse, and the system's response after dynamical evolution is detected by another delayed probe pulse. The observed TA PP signal thus reflects the third-order response of the system on the laser fields of the pump and probe pulses, which gives the spectral fingerprint of the system dynamics governed by the time-dependent evolution of the density operators.[21−23]

In recent years, the trajectory-based on-the-fly *ab initio* nonadiabatic dynamics simulations have been used extensively to investigate the ultrafast nonradiative electronic decay in polyatomic systems.[4,24−26] Most on-the-fly nonadiabatic simulations focus on recording the dynamics evolution in the photoinduced processes. Correspondingly, their results give rich information related to time-dependent molecular geometries, energies, and electronic-state populations. Comparatively little attention has been paid to the simulations of experimentally measured time-resolved signals on the basis of on-the-fly nonadiabatic dynamics, although several methods and protocols have been developed for the simulation of PP-like signals. *Ab initio* simulations of time-resolved PP photoelectron spectra were carried out by using classical-trajectory guided Gaussian basis set method and semiclassical Wigner representation method.[3,27] In these simulations, one evaluates, in fact, excited-state absorption (ESA) contribution to the TA PP signal, which yields projection of the vibronic wavepacket in the lower-lying electronic states to the cationic product state. The time-resolved fluorescence spectrum, which has been simulated by employing the Einstein coefficient approach,[28−33] is proportional to the stimulated-emission (SE) contribution to the TA PP spectrum. On-the-fly simulations of TA PP spectra were performed by employing the cumulant/harmonic approximation for vibrational contributions,[34−36] single-Gaussian-wavepacket Ansatz,[37] and real-time time-dependent density-functional theory methodology.[38−40] In

Received: October 14, 2021
Accepted: December 15, 2021
Published: January 13, 2022

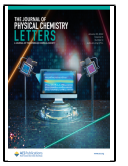

https://doi.org/10.1021/acs.jpclett.1c03373
J. Phys. Chem. Lett. 2022, 13, 661−668

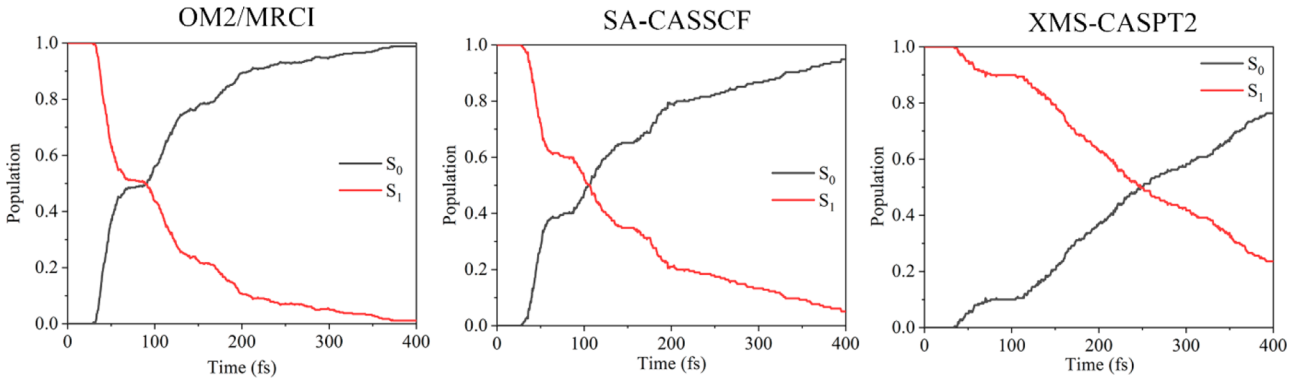

Figure 1. Time-dependent fractional occupations of the S_0 and S_1 electronic states of AZM in nonadiabatic dynamics staring from the S_1 state. A total of 200 trajectories were used for obtaining the converged results.

the aforementioned simulation methods simplifying assumptions are unavoidable, since one must approximate essentially quantum dynamics of the molecular system driven by external fields by evolution along classical trajectories. Hence novel approaches and protocols, notably those allowing the on-the-fly simulation of TA PP signals with realistic pulse envelopes are still necessary. For instance, Gelin, Domcke, and coworkers recently proposed a practical approach to simulate the TA PP signals by combing the on-the-fly trajectory simulation and the doorway-window (DW) representation of nonlinear spectroscopy.[41]

While the development of the universally applicable and reliable tools for the simulation of TA PP signals of polyatomic chromophores and molecular aggregates is certainly challenging, the other theoretical issue is also significant in applications of such simulations to specific molecular systems, for instance to address the important role of the non-Condon effects and the nonadiabatic decay to the electronic ground state in the explanation of time-resolved TA PP spectra. At the same time, it is well-known that nonadiabatic dynamics simulations with different electronic structure methods often deliver different or even contradictory results.[42,43] However, benchmarking of time-resolved TA PP spectra simulated at various quantum-chemistry levels is still lacking. Herein, one aim of this work is to investigate the performance of three different electronic structure methods in the nonadiabatic dynamics simulation of TA PP spectra and in the monitoring of internal conversion (IC) to the electronic ground state. For this purpose, we extended the on-the-fly trajectory simulation of the TA PP signal within the DW approximation by including the IC to the ground state, which plays an essential role in photochemistry and photophysics.

The nonadiabatic dynamics of azomethane (AZM in Figure S1) and the TA PP signals were studied by on-the-fly *ab initio* nonadiabatic trajectory surface hopping (TSH) dynamic simulations[44] at three different electronic structure levels. The orthogonalization-corrected OM2 Hamiltonian combined with multireference configuration interaction (OM2/MRCI),[45] the state averaged complete active space self-consistent field (SA-CASSCF),[46,47] and extended multistate multireference second-order perturbation theory (XMS-CASPT2)[48] methods were employed here because they can well describe the topology of S_0/S_1 potential energy surfaces. As AZM is the simplest azoalkane, the study of photodynamics processes in this molecule has attracted considerable attention.[49−53] The first low-lying $n-\pi^*$ excited state was found to play a crucial role in the photoinduced decay. Many experimental and theoretical studies have been conducted to investigate the photoinduced dynamics of AZM after photoexcitation. It was scrutinized by femtosecond-multiphoton spectroscopy,[54] nanosecond-coherent antistokes Raman spectroscopy,[55] *ab initio* potential energies surface calculation, and dynamics simulation.[53,56,57]

We wish to study which information can be obtained from the population dynamics and time-resolved TA PP signals simulated for AZM on-the-fly, as well as to clarify the role of the non-Condon effects. As is well-known, AZM exists in two isomers, *cis*-AZM and *trans*-AZM. In this work, we focus on the former due to the following considerations. To make the present study clean and clear, the ideal prototypical system should exhibit IC from the first excited state S_1 to the ground state S_0. Here we prefer not to include the higher excited state in the model study, because the time-resolved TA PP signals may vanish due to the IC between the excited states if the lower excited state displays much smaller transition dipole moments (TDMs). Thus, we simply choose *cis*-azomethane that shows the larger $S_0 \rightarrow S_1$ TDM and focus on the study of the $S_1 \rightarrow S_0$ IC and the associated time-resolved TA PP signals. Several works have discussed the photoinduced dynamics of *cis*-AZM.[51−53,57]

In the present work, the TA PP signals were simulated with the DW representation of the nonlinear response.[21,41,58−62] This method, which is valid if the pump and probe pulses are temporally well separated, allows one to fully account for realistic pulse shapes in the time and frequency domain. The theoretical aspects of the method and interfacing of the DW representation and the TSH simulation procedure were discussed in refs 41 and 63. In short, the DW representation casts TA PP signals in terms of vibronic wavepackets. However, additional approximations are necessary to represent overlaps of quantum D and W wavepackets in terms of classical trajectories. These approximations include the classical Condon approximation, replacement of quantum dynamics by the TSH dynamics, and substitution of quantum averaging by averaging over classical trajectories sampled from the Wigner distribution. With these approximations, TA PP signals are fully expressed through the TDMs and electronic energies which are evaluated along the TSH trajectories. In this work, the DW framework of ref 41 is extended to account for the $S_1 \rightarrow S_0$ IC, thereby allowing that trajectories in the lowest excited electronic state S_1 jump to the ground electronic state S_0 (see Supporting Information for all theoretical and

https://doi.org/10.1021/acs.jpclett.1c03373
J. Phys. Chem. Lett. 2022, 13, 661−668

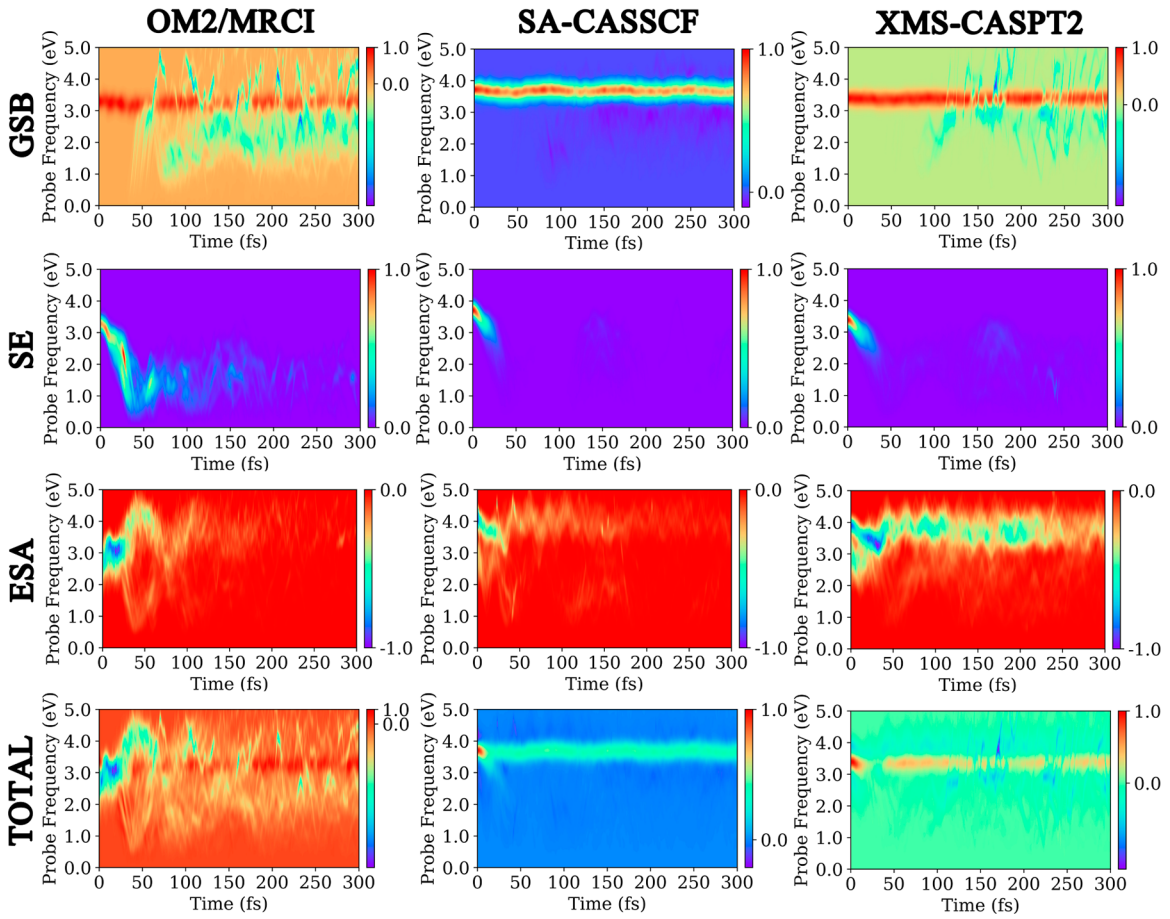

Figure 2. Normalized GSB, SE, and ESA contributions and total integral TA PP signal of AZM as a function of the pump−probe delay time τ and the central frequency ω_{pr} of the probe pulse. Duration of both pump and probe pulses is 5 fs. The central frequency ω_{pu} of the pump pulse is tuned into resonance with the $S_1(n\pi^*)$ state (OM2/MRCI, 3.37 eV; SA-CASSCF, 3.70 eV; XMS-CASPT2, 3.40 eV). (Left column) OM2/MRCI method, (middle column) SA-CASSCF method, (right column) XMS-CASPT2 method.

computational details). Then we study how the simulated photoinduced dynamics and TA PP spectra depend on the use of different levels of electronic-structure theories.

We begin with the population dynamics in Figure 1, which shows the time-dependent fractional occupations of the S_0 and S_1 electronic states of AZM, assuming that all trajectories started from the S_1 state. Very similar population evolutions are obtained at OM2/MRCI and SA-CASSCF levels, giving the 50% S_1 decay around 91 and 105 fs, respectively. At 400 fs, the S_1 population becomes very low, and the $S_1 \rightarrow S_0$ IC is essentially over. However, the TSH dynamics at the XMS-CASPT2 level yields a much longer time scale (249 fs) of the 50% S_1 population decay. At 400 fs, more than 20% of the population remains in the S_1 state. In our work, the isomerization yields from *cis* to *trans* are 0.30 (OM2/MRCI), 0.53 (SA-CASSCF), and 0.53 (XMS-CASPT2), respectively. The latter two agree well with the result (0.55) obtained in ref 53 (see Table S3).

Next, let us consider TA PP signals. It is appropriate to start from the qualitative picture of the formation of these signals in AZM. The total TA PP signal can be decomposed into three contributions, the ground-state bleach (GSB), SE, and ESA. With the inclusion of IC, these contributions are calculated in the DW formalism as follows. At $t = 0$, the pump pulse creates the D-wavepackets in the states S_0 and S_1. Then, classical trajectories are propagated in the states S_0 and S_1 up $t = \tau$ where τ is the time delay between the pump and probe pulses. At $t = \tau$, the probe pulse creates the W-wavepackets, which probe the nuclear motion in the state S_0 through the $S_0 \rightarrow S_1$ optical transitions (GSB) and in the state S_1 through the $S_1 \rightarrow S_0$ (SE) and $S_1 \rightarrow$ higher-lying states' (ESA) optical transitions. Finally, the TA PP signal is obtained by averaging the product of the D-wavepacket at $t = 0$ and the W-wavepacket at $t = \tau$ over nuclear trajectories.[41] Within the TSH picture, a trajectory contributes to the SE and ESA signals only when it propagates in the excited state S_1. When the trajectory jumps back to the ground state S_0, its contribution to the SE and ESA signals vanishes while the contribution to the GSB signal emerges. Hence, the GSB signal consists of two components. The first (hereafter "cold") component is the conventional GSB signal which reflects the evolution of the hole wavepacket created and probed in S_0. The second (hereafter "hot") component describes the wavepackets which are launched by the pump pulse into S_1, undergo $S_1 \rightarrow S_0$ IC, and are interrogated by the probe pulse in S_0. As explained in the Supporting Information, the two components of the GSB signal have opposite signs. Following the convention used in the present work, the cold GSB and the SE signals are positive, while the hot GSB and the ESA are negative.

In the simulation of TA PP signals, the pump and probe pulses with Gaussian envelopes $E(t) = \exp\{-(t/\tau_p)^2\}$ were used. The pulse durations for both the pump and probe pulses

https://doi.org/10.1021/acs.jpclett.1c03373
J. Phys. Chem. Lett. 2022, 13, 661−668

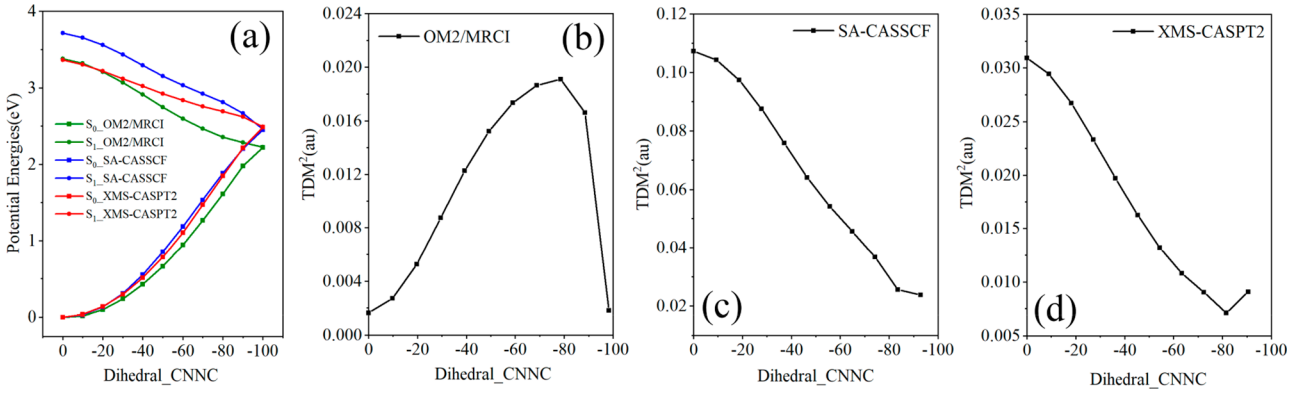

Figure 3. Potential energy curves (a), S_0−S_1 TDMs squared, and the highest occupied molecular orbitals (contributing to the electronic transition in the S_1 state) along the linear interpolated pathway from S_0_min to the conical intersection (b−d), calculated by the electronic-structure methods indicated in the legends.

are set to 5 fs, which yields the bandwidth of 0.44 eV (full width at half-maximum). The GSB, SE, and ESA contributions as well as the total integral TA PP signal within the first 300 fs are shown in Figure 2. To enhance the short-time features, the same signals are depicted on the time scale of 50 fs in Figure S2.

The GSB signals are plotted in the upper panels of Figure 2. As explained above, the GSB signals consist of two components. The cold (positive) component is almost stationary. It is located around ω_{pr} ∼3.4 eV (OM2/MRCI), 3.7 eV (SA-CASSCF), and 3.4 eV (XMS-CASPT2). The hot (negative) high-amplitude component emerges around 50 fs (OM2/MRCI) and 100 fs (XMS-CASPT2) and oscillates around the cold component.

The SE contribution (middle panels) directly reflects the wavepacket evolution in the S_1 state. The SE spectra computed at the SA-CASSCF and XMS-CASPT2 levels are relatively similar, except for the different original emission positions. Let us take the SA-CASSCF signal as an example. The excited-state trajectories are initiated in the $S_1(n\pi^*)$ state, because the excitation energy of this state is assumed to be in resonance with the central frequency of the pump pulse. The signal moves to the lower frequencies, significantly weakens already at $\tau \sim 10$ fs, and almost vanishes at $\tau \sim 30$ fs. However, OM2/MRCI provides a different evolution of the SE component. Within the first 20 fs the SE signal moves to the lower frequencies, and its intensity becomes slightly weaker. However, within 25−40 fs, the SE intensity shows a recurrence and then decays almost completely on the time scale of around 150 fs. During this evolution, the SE signal shifts to the low-energy domain.

The ESA signals reflect the electronic transitions from the lower-lying excited states (in which excited-state wavepacket dynamics takes place) to the optically allowed higher-lying excited states. It is not trivial to simulate ESA spectra, as the excitation from the current dynamically relevant excited state to higher-lying excited states must be calculated. Hence the ESA contributions presented in Figure 2 and Figure S2 can be regarded as semiquantitative, since they are calculated by using snapshots taken from the trajectory propagation and performing the additional single-point calculations of four electronic states at the individual electronic-structure level. The ESA signals given at the OM2/MRCI level are slightly red-shifted in the very beginning and then exhibit the significant blue shift by ∼1.5 eV at $\tau > 50$ fs. This indicates that the optically allowed electronic transition from the S_1 to higher-lying excited states becomes possible along the trajectory. When more trajectories jump back to the electronic ground state, the ESA signal almost disappears at $\tau > 200$ fs. At the SA-CASSCF and XMS-CASPT2 levels, different ESA signals are obtained, while both spectral shift and intensity decay are given within 50 fs. The ESA signals vanish in the longer time scale owing to the $S_1 \rightarrow S_0$ IC. At the XMS-CASPT2 level, the nonadiabatic population decay is slower than that at the other two levels (see Figure 1) and the corresponding ESA signal also vanishes on the longer time scale. The significant differences in the ESA signals are attributed to the fact that the high-lying excited states responsible for the ESA signals significantly depend on the level of electronic structure theories. It is well-known that such dependence represents a great challenge in quantum chemistry.

The total integral signal is the sum of the GSB, SE, and ESA contributions, as depicted in Figure 2 and Figure S2. The OM2/MRCI TA PP spectrum is initially dominated by the ESA signal, but later also exhibits clear hot and cold GSB contributions. The SA-CASSCF signal is dominated by the cold GSB contribution, and the XMS-CASPT2 signals exhibit pronounced GSB and ESA contributions. It is important that the SA-CASSCF and XMS-CASPT2 spectra in the low energy region are similar, and the early time decaying (at ∼20 fs) SE contributions may be extracted from the total TA PP signal, when we consider the frequency shift of the SE signal.

No matter which electronic structure methods are used, both on-the-fly TSH nonadiabatic dynamics and time-resolved TA PP signals indicate that the IC in AZM takes place on the ultrafast time scale. However, the detailed comparison of the nonadiabatic population dynamics in Figure 1 and the TA PP signals in Figure 2 reveal a number of interesting questions. For example, OM2/MRCI and SA-CASSCF give similar population dynamics, while the corresponding TA PP spectra differ substantially. At the same time, SA-CASSCF and XMS-CASPT2 predict noticeably different S_0 and S_1 population evolutions, but the corresponding TA PP signals, in particular the GSB and SE components, show many similarities. In addition, simulations at all three levels of electronic structure theory predict that the SE signals decay much faster than the S_1 populations. Usually, it is assumed that the time-resolved SE signal directly reflects the nonadiabatic population decay, while our results indicate that the two observables are not equivalent for AZM. In what follows we analyze all these intriguing problems in detail.

https://doi.org/10.1021/acs.jpclett.1c03373
J. Phys. Chem. Lett. 2022, 13, 661−668

To understand the difference between the predictions of the three electronic structure methods, the reaction pathway from the ground-state minimum (S_0_min) to the conical intersection was built by employing the linear interpolated method, and the corresponding potential energy curves as functions of the dihedral angle C−N−N−C obtained by the three methods are presented in Figure 3a. The three methods predict that the barrierless pathways on the S_1 potential energy curve connect the Franck−Condon (FC) point with the S_0/S_1 conical intersection. As a function of the torsional angle, the XMS-CASPT2 pathway is flatter compared to the OM2/MRCI and SA-CASSCF pathways. This clearly explains why the TSH dynamics at the XMS-CASPT2 level predicts the longer S_1 excited state lifetime. The S_0_min geometry and the excited state properties at S_0_min are given in the Supporting Information.

The calculated TDMs between the S_0 and S_1 states along the linear-interpolated excited-state reaction pathway from the ground state minimum to the S_0/S_1 conical intersection are given in panels (b−d) of Figure 3. As discussed above, the linear interpolated potential energy curves calculated by the three methods are quite close to each other. However, the S_0−S_1 TDMs depend dramatically on the chosen levels of the electronic structure theories. For instance, both SA-CASSCF and XMS-CASPT2 methods predict that the TDM decreases monotonically with the C−N−N−C dihedral angle from the FC region to the S_0/S_1 conical intersection. As shown in Figure S3, at the FC region, the S_1 state is characterized by the HOMO (n)−LUMO (π^*) transition. With the C−N−N−C torsional motion, both HOMO and LUMO orbitals display more localized p-type orbital characters. The overlap between their densities decreases significantly, and thus the $S_0 \rightarrow S_1$ TDM decays dramatically with this torsional coordinate. At the XMS-CASPT2 level, the SA-CASSCF wave function of the S_1 state is perturbed by the low-lying excited states not far from S_1. Both S_2 and S_3 states display much weaker TDM, and thus the dark transition components should be added into the S_1 state. This explains the smaller $S_0 \rightarrow S_1$ TDM at the XMS-CASPT2 level. The different dependence of the TDM on the torsional angle was obtained at the OM2/MRCI level. The HOMO orbital displays more significant $n-\sigma$ mixing at the OM2/MRCI level. Since the σ component has much lower overlap with the π^* orbital density, the $S_0 \rightarrow S_1$ TDM at the Franck−Condon region is much smaller. With the C−N−N−C torsional motion, such $n-\sigma$ mixing starts to disappear, and the transition becomes closer to the $n-\pi^*$ transition. Later, the localized p-type orbital character comes out again. This explains the initial rise and later decay of the $S_0 \rightarrow S_1$ TDM as a function of the C−N−N−C torsional motion. The different $S_0 \rightarrow S_1$ TDM features and the non-Condon effects described clearly explain the remarkable differences in the SE and GSB signals obtained at the OM2/MRCI, SA-CASSCF, and XMS-CASPT2 levels.

Let us now discuss the SE component of the TA PP signal. In the early stage of the dynamics, the trajectory experiences the torsional motion of the CNNC dihedral angle on the S_1 potential energy surface, as shown in Figure S4. Both the SA-CASSCF and XMS-CASPT2 predict that the TDMs decrease dramatically due to the fast CNNC torsional motion. Along this torsional motion, the S_0−S_1 energy gap also becomes smaller. As a consequence, the SE signals first appear in the FC region at the beginning of the nonadiabatic dynamics and then move to the lower-energy domain. At the same time the SE intensity becomes weaker and quickly vanishes when the trajectory enters the regions in which the TDMs become rather small. We also noticed that the vanishing of the TDM values begins much earlier than when the trajectories access the S_0/S_1 conical intersection. Therefore, the SE signals quench much earlier than the S_1 populations. When the trajectory is propagated at the OM2/MRCI level, the torsional motion increases the TDM and decreases the S_0−S_1 energy gap. Thus, the SE signal moves to the low-frequency domain in this early stage. Although the TDM increases, different trajectories start to spread over a broad area in the phase space, and these trajectories show different transition energies. As the result, the SE intensity does not increase significantly. When most trajectories move close to the geometries with larger TDMs at a CNNC dihedral angle of ∼60° at about 25 fs, the recurrence of the SE appears in the low-energy domain. Next the trajectories move to the regions with small S_0−S_1 TDM at 30−40 fs and the SE signal starts vanishing. As distinct from the SA-CASSCF and XMS-CASPT2 results, the recurrence of the SE signal is also attributed to the nonvanishing S_0−S_1 TDM along the torsional motion at the OM2/MRCI level. Overall, the differences discussed here indicate that the OM2/MRCI method may not be accurate enough to describe the excited-state electronic wave function and TDM for the current system, even if the state energy may be reasonable.

The time-dependent state population decay is governed exclusively by the profiles of the excited-state pathways. The SE signal quenches both due to the vanishing of TDMs in certain areas of the nuclear phase space and the IC to the ground state. This explains why the SE signals decay much faster than the nonadiabatic populations and demonstrates the nontrivial interconnection between the nonadiabatic dynamics and the TA PP signal evolution.

Next, let us analyze the GSB signal in details. The "cold" component in the GSB signal is relevant to the dynamics of the "hole" created by the D-wavepacket. The weak modulation here is caused by the combination of non-Condon effects in the FC region (Figure S5), anharmonic effects, and finite pulse duration. The "hot" GSB signal is governed by the interplay between the "hot" vibrational motion and the strong dependence of the S_1−S_0 TDM on nuclear coordinates (Figure 3). The S_1−S_0 TDM decreases dramatically with the torsional motion at the SA-CASSCF and XMS-CASPT2 levels. It should be noted that the current simulations are performed for isolated AZM. Hence the excessive energies drive the large-amplitude nuclear motion, and the spreading of the $S_1 \rightarrow S_0$ trajectories in the phase space makes the hot component of the GSB signal quite erratic. We noticed that the CN bond cleavage may take place in the ground state after the IC, at OM2/MRCI and XMS-CASPT2 levels, as shown in the Supporting Information. Consistent with the work by Sellner et al.,[53] our result indicates that the barrierless excited-state pathways from the FC region to the CI are dominated by the CNNC torsion, and the dissociation processes are energetically accessible after the IC. The existence of the CN dissociation may have substantial influence on the time-resolved signals. Since the CN bond breaking mainly takes place on the ground state, we expected that it does not affect the SE and ESA signals. However, it does influence the GSB signals. In some situations, two GSB components may cancel each other and the total GSB signal should eventually disappear when the system fully returns back to the ground state minimum and

https://doi.org/10.1021/acs.jpclett.1c03373
J. Phys. Chem. Lett. 2022, 13, 661−668

becomes completely thermalized. This vibrational cooling may occur on a much longer (from tens to hundreds of picoseconds) time scale. However, in the current situation, the isomerization and CN dissociation processes prevent the recovery of initial conditions, and the total GSB signals do not vanish. After the IC, more CN dissociation takes place at the OM2/MRCI and XMS-CASPT2 levels, and the resulting GSB signals become more chaotic, as shown in Figure 2.

The ESA signal is relevant to the optically allowed transition from the S_1 state to the higher excited state. Here only the low-lying S_2 and S_3 states are considered, the transition properties of which along the reaction pathway are given in Tables S4–S6. Since these results are rather qualitative and strongly dependent on the electronic structure levels, we do not give the detailed analysis here. But we need to point out that the ESA vanish can be regarded as a signature of the IC.

It is crucial that the results of the population dynamic simulations and the TA PP spectral simulations, taken together, give logically consistent and fairly complete information on the photoinduced processes in AZM at any level of the electronic structure theory. The following qualitative picture emerges which can be dissected into three steps. (i) The S_1 state is populated from the ground state in the FC region by the pump pulse and the excited-state wavepacket moves downhill toward lower energies, away from the FC region of the S_1 potential energy surface to the area with low values of the S_0−S_1 TDMs. This step is manifested through the SE signal which quenches on the time scale of several tens of femtoseconds (depending on a specific electronic structure method) when the wavepacket enters (almost) the optically dark area of the S_1 state. It is important that the SE signal does not correspond to the S_1 population dynamics, because the wavepacket remains in the S_1 potential energy surface. However, the vanishing of the SE signal directly reflects the time scale at which the wavepacket moves from the FC region. (ii) The arrival of the S_1 wavepacket to the low-energy region of the S_1 potential energy surface triggers the $S_1 \rightarrow S_0$ IC which is manifested as a hot (negative) GSB wavepacket which exhibits high-amplitude oscillations in the time domain. (iii) The region of the S_1 potential energy surface with weak S_0−S_1 TDMs possesses strong TDMs from the S_1 to higher-lying electronic states. Thus, the ESA can be considered as a reporter of the depopulation of the S_1 state, and the ESA quenching times roughly coincide with the lifetimes of electronic populations in Figure 1. The onset of the ESA, on the other hand, depends significantly on the electronic structure method employed.

In conclusion, we report the on-the-fly nonadiabatic dynamics simulation of electronic populations and time-resolved TA PP spectra for azomethane. Three different electronic-structure theories are used in the TSH nonadiabatic dynamics simulations. Both OM2/MRCI and SA-CASSCF methods give similar lifetimes of the S_1 excited state, while a much longer lifetime is obtained at the XMS-CASPT2 level. This is consistent with the energy profile of the excited-state reaction pathway from the FC region to the conical intersection. In the simulated TA PP spectra, the SA-CASSCF and XMS-CASPT2 methods give very similar SE signals, and the SE quenching is caused by the decrease of the S_0−S_1 TDM along the reaction coordinate, that is, the CNNC torsion. The OM2/MRCI SE signal is quite different due to the qualitatively different dependence of the TDM on the CNNC torsional angle. The ESA can be regarded as a signature of the IC, since the ESA quenching indicates the completion of the $S_1 \rightarrow S_0$ IC. However, the simulated ESA signals are strongly dependent on the chosen excited-state methods, and this represents a great challenging topic in the electronic-structure theory. Overall, it is demonstrated that electronic populations and time-resolved TA PP signals may reflect different information on the photoinduced excited-state processes. We uncover microscopic reasons for that and establish connections between nonadiabatic dynamics and time-resolved spectroscopic signals. These connections create a bridge between experimental observations and theoretical simulations and deepen our understanding of the formation of time-resolved spectra.

The present work has two important messages. First, the employment of different electronic-structure theories can deeply influence not only the electronic population evolutions but also time-resolved TA PP spectra. Furthermore, different electronic-structure methods can have different impacts on these two classes of observables, because evolutions of excited-states populations and SE signals reveal different aspects of the photophysical processes: the population dynamics is governed by the potential energy surface and its gradient, while the TA PP spectrum depends, additionally, on the TDMs. This strongly indicates that it is not enough to take the population dynamics as the reference data to examine the performance of excited-state electronic-structure methods. The simulation of the time-resolved spectroscopic signals provides another important dimension to validate the accuracy of the quantum chemistry methods. Second, TA PP signals may be strongly affected by time-dependent changes of TDMs caused by non-Condon effects, which should be considered to properly understand the time-resolved TA PP signals obtained from the nonadiabatic dynamics simulation involving the large amplitude nuclear motions in polyatomic systems. Overall, the cohesive combination of the *ab initio* simulation of nonadiabatic dynamics and ultrafast spectroscopic signals can provide a powerful tool to predict and interpret experimental observables, as well as reveal the photoinduced reactions and photophysical mechanisms behind the ultrafast excited-state processes.

■ ASSOCIATED CONTENT

Supporting Information

The Supporting Information is available free of charge at https://pubs.acs.org/doi/10.1021/acs.jpclett.1c03373.

Theoretical methods, S_0 minimum-energy molecular geometry, TDM at S_0 minimum, isomerization yields, transition energies and TDM along the linear interpolated pathway from S_0_min to the conical intersection at three methods, GSB, SE, and ESA contributions within 50 fs, HOMO and LUMO at different geometries from S_0_min to the CI, time-dependent CNNC dihedral angle distribution in first 100 fs dynamics with different dynamics methods, potential energy curves and TDMs as functions of the NN distance, the distribution of C−N distance at hopping geometries, the C−N distance along with the trajectories evolution, the possible IC pathways from the Franck−Condon region of AZM (*trans* and *cis* isomers) to the CI and consecutive dissociation pathway of one methyl group, and the dispersed GSB, SE, and ESA contributions and total signals, and additional implementation details (PDF)

https://doi.org/10.1021/acs.jpclett.1c03373
J. Phys. Chem. Lett. 2022, 13, 661−668

AUTHOR INFORMATION

Corresponding Author

Zhenggang Lan − *Guangdong Provincial Key Laboratory of Chemical Pollution and Environmental Safety and MOE Key Laboratory of Environmental Theoretical Chemistry, SCNU Environmental Research Institute, School of Environment, South China Normal University, Guangzhou 510006, P. R. China;* orcid.org/0000-0002-8509-0388; Email: zhenggang.lan@m.scnu.edu.cn, zhenggang.lan@gmail.com

Authors

Chao Xu − *Key Laboratory of Theoretical Chemistry of Environment, Ministry of Education; School of Chemistry, South China Normal University, Guangzhou 510006, P. R. China;* orcid.org/0000-0002-4043-2954

Kunni Lin − *Key Laboratory of Theoretical Chemistry of Environment, Ministry of Education; School of Chemistry, South China Normal University, Guangzhou 510006, P. R. China;* orcid.org/0000-0001-6591-8953

Deping Hu − *Guangdong Provincial Key Laboratory of Chemical Pollution and Environmental Safety and MOE Key Laboratory of Environmental Theoretical Chemistry, SCNU Environmental Research Institute, School of Environment, South China Normal University, Guangzhou 510006, P. R. China;* orcid.org/0000-0001-7161-1253

Feng Long Gu − *Key Laboratory of Theoretical Chemistry of Environment, Ministry of Education; School of Chemistry, South China Normal University, Guangzhou 510006, P. R. China;* orcid.org/0000-0002-8141-6774

Maxim F. Gelin − *School of Sciences, Hangzhou Dianzi University, Hangzhou 310018, P. R. China;* orcid.org/0000-0003-3092-3343

Complete contact information is available at: https://pubs.acs.org/10.1021/acs.jpclett.1c03373

Notes

The authors declare no competing financial interest.

ACKNOWLEDGMENTS

This work is supported by NSFC projects (No. 21933011, 21873112, 21673266, and 21903030). The authors thank the Supercomputing Center, Computer Network Information Center, Chinese Academy of Sciences. M.F.G. acknowledges support from Hangzhou Dianzi University through startup funding.

REFERENCES

(1) Domcke, W.; Yarkony, D.; Köppel, H. *Conical intersections: electronic structure, dynamics & spectroscopy*; World Scientific: 2004; Vol. *15*.

(2) Domcke, W.; Yarkony, D. R.; Köppel, H. *Conical intersections: theory, computation and experiment*; World Scientific: 2011; Vol. *17*.

(3) Curchod, B. F.; Martínez, T. J. Ab initio nonadiabatic quantum molecular dynamics. *Chem. Rev.* **2018**, *118* (7), 3305−3336.

(4) Crespo-Otero, R.; Barbatti, M. Recent advances and perspectives on nonadiabatic mixed quantum-classical dynamics. *Chem. Rev.* **2018**, *118* (15), 7026−7068.

(5) Cheng, Y.-C.; Fleming, G. R. Dynamics of light harvesting in photosynthesis. *Annu. Rev. Phys. Chem.* **2009**, *60*, 241−262.

(6) Gozem, S.; Luk, H. L.; Schapiro, I.; Olivucci, M. Theory and simulation of the ultrafast double-bond isomerization of biological chromophores. *Chem. Rev.* **2017**, *117* (22), 13502−13565.

(7) Szymanski, W.; Beierle, J. M.; Kistemaker, H. A.; Velema, W. A.; Feringa, B. L. Reversible photocontrol of biological systems by the incorporation of molecular photoswitches. *Chem. Rev.* **2013**, *113* (8), 6114−6178.

(8) Bandara, H. D.; Burdette, S. C. Photoisomerization in different classes of azobenzene. *Chem. Soc. Rev.* **2012**, *41* (5), 1809−1825.

(9) Segatta, F.; Cupellini, L.; Garavelli, M.; Mennucci, B. Quantum Chemical Modeling of the Photoinduced Activity of Multichromophoric Biosystems: Focus Review. *Chem. Rev.* **2019**, *119* (16), 9361−9380.

(10) Curutchet, C.; Mennucci, B. Quantum chemical studies of light harvesting. *Chem. Rev.* **2017**, *117* (2), 294−343.

(11) Middleton, C. T.; de La Harpe, K.; Su, C.; Law, Y. K.; Crespo-Hernandez, C. E.; Kohler, B. DNA Excited-State Dynamics: From Single Bases to the Double Helix. *Annu. Rev. Phys. Chem.* **2009**, *60* (1), 217−239.

(12) Crespo-Hernández, C. E.; Cohen, B.; Hare, P. M.; Kohler, B. Ultrafast excited-state dynamics in nucleic acids. *Chem. Rev.* **2004**, *104* (4), 1977−2020.

(13) Dantus, M. COHERENT NONLINEAR SPECTROSCOPY: From Femtosecond Dynamics to Control. *Annu. Rev. Phys. Chem.* **2001**, *52* (1), 639−679.

(14) Pollard, W. T.; Mathies, R. A. Analysis of femtosecond dynamic absorption spectra of nonstationary states. *Annu. Rev. Phys. Chem.* **1992**, *43* (1), 497−523.

(15) Kowalewski, M.; Fingerhut, B. P.; Dorfman, K. E.; Bennett, K.; Mukamel, S. Simulating coherent multidimensional spectroscopy of nonadiabatic molecular processes: From the infrared to the x-ray regime. *Chem. Rev.* **2017**, *117* (19), 12165−12226.

(16) Maiuri, M.; Garavelli, M.; Cerullo, G. Ultrafast spectroscopy: State of the art and open challenges. *J. Am. Chem. Soc.* **2020**, *142* (1), 3−15.

(17) Conti, I.; Cerullo, G.; Nenov, A.; Garavelli, M. Ultrafast spectroscopy of photoactive molecular systems from first principles: Where we stand today and where we are going. *J. Am. Chem. Soc.* **2020**, *142* (38), 16117−16139.

(18) Polley, K.; Loring, R. F. Two-dimensional vibrational-electronic spectra with semiclassical mechanics. *J. Chem. Phys.* **2021**, *154* (19), 194110.

(19) Gao, X.; Geva, E. A nonperturbative methodology for simulating multidimensional spectra of multiexcitonic molecular systems via quasiclassical mapping Hamiltonian methods. *J. Chem. Theory Comput.* **2020**, *16* (10), 6491−6502.

(20) Yan, Y.; Liu, Y.; Xing, T.; Shi, Q. Theoretical study of excitation energy transfer and nonlinear spectroscopy of photosynthetic light-harvesting complexes using the nonperturbative reduced dynamics method. *Wiley Interdiscip. Rev. Comput. Mol. Sci.* **2021**, *11* (3), e1498.

(21) Mukamel, S. *Principles of nonlinear optical spectroscopy*; Oxford University Press on Demand: 1999.

(22) Gelin, M. F.; Egorova, D.; Domcke, W. Efficient calculation of time-and frequency-resolved four-wave-mixing signals. *Acc. Chem. Res.* **2009**, *42* (9), 1290−1298.

(23) Domcke, W.; Stock, G. Theory of ultrafast nonadiabatic excited-state processes and their spectroscopic detection in real time. *Adv. Chem. Phys.* **2007**, *100*, 1−169.

(24) Du, L.; Lan, Z. An on-the-fly surface-hopping program jade for nonadiabatic molecular dynamics of polyatomic systems: implementation and applications. *J. Chem. Theory Comput.* **2015**, *11* (4), 1360−1374.

(25) Mai, S.; González, L. Molecular photochemistry: Recent developments in theory. *Angew. Chem., Int. Ed.* **2020**, *59* (39), 16832−16846.

(26) Barbatti, M.; Granucci, G.; Persico, M.; Ruckenbauer, M.; Vazdar, M.; Eckert-Maksić, M.; Lischka, H. The on-the-fly surface-hopping program system Newton-X: Application to ab initio simulation of the nonadiabatic photodynamics of benchmark systems. *J. Photochem. Photobiol., A* **2007**, *190* (2−3), 228−240.

(27) Bonačić-Koutecký, V.; Mitrić, R. Theoretical exploration of ultrafast dynamics in atomic clusters: Analysis and control. *Chem. Rev.* **2005**, *105* (1), 11−66.
(28) Cusati, T.; Granucci, G.; Persico, M. Photodynamics and time-resolved fluorescence of azobenzene in solution: a mixed quantum-classical simulation. *J. Am. Chem. Soc.* **2011**, *133* (13), 5109−5123.
(29) Klaumünzer, B.; Kröner, D.; Lischka, H.; Saalfrank, P. Non-adiabatic excited state dynamics of riboflavin after photoexcitation. *Phys. Chem. Chem. Phys.* **2012**, *14* (24), 8693−8702.
(30) Lan, Z.; Lu, Y.; Weingart, O.; Thiel, W. Nonadiabatic decay dynamics of a benzylidene malononitrile. *J. Phys. Chem. A* **2012**, *116* (6), 1510−1518.
(31) Pang, X.; Cui, X.; Hu, D.; Jiang, C.; Zhao, D.; Lan, Z.; Li, F. Watching" the dark state in ultrafast nonadiabatic photoisomerization process of a light-driven molecular rotary motor. *J. Phys. Chem. A* **2017**, *121* (6), 1240−1249.
(32) Roy, S.; Ardo, S.; Furche, F. 5-methoxyquinoline photobasicity is mediated by water oxidation. *J. Phys. Chem. A* **2019**, *123* (31), 6645−6651.
(33) Yu, J. K.; Liang, R.; Liu, F.; Martínez, T. J. First-principles characterization of the elusive i fluorescent state and the structural evolution of retinal protonated schiff base in bacteriorhodopsin. *J. Am. Chem. Soc.* **2019**, *141* (45), 18193−18203.
(34) Polli, D.; Altoe, P.; Weingart, O.; Spillane, K. M.; Manzoni, C.; Brida, D.; Tomasello, G.; Orlandi, G.; Kukura, P.; Mathies, R. A.; Garavelli, M.; Cerullo, G. Conical intersection dynamics of the primary photoisomerization event in vision. *Nature* **2010**, *467* (7314), 440−443.
(35) Segarra-Martí, J.; Mukamel, S.; Garavelli, M.; Nenov, A.; Rivalta, I. Towards accurate simulation of two-dimensional electronic spectroscopy. *Multidimensional time-resolved spectroscopy* **2019**, 63−112.
(36) Segatta, F.; Nenov, A.; Nascimento, D. R.; Govind, N.; Mukamel, S.; Garavelli, M. iSPECTRON: A simulation interface for linear and nonlinear spectra with ab-initio quantum chemistry software. *J. Comput. Chem.* **2021**, *42* (9), 644−659.
(37) Begušić, T.; Roulet, J.; Vaníček, J. On-the-fly ab initio semiclassical evaluation of time-resolved electronic spectra. *J. Chem. Phys.* **2018**, *149* (24), 244115.
(38) Nguyen, T. S.; Koh, J. H.; Lefelhocz, S.; Parkhill, J. Black-box, real-time simulations of transient absorption spectroscopy. *J. Phys. Chem. Lett.* **2016**, *7* (8), 1590−1595.
(39) Bonafé, F. P.; Hernández, F. J.; Aradi, B. l.; Frauenheim, T.; Sánchez, C. n. G. Fully atomistic real-time simulations of transient absorption spectroscopy. *J. Phys. Chem. Lett.* **2018**, *9* (15), 4355−4359.
(40) Krumland, J.; Valencia, A. M.; Pittalis, S.; Rozzi, C. A.; Cocchi, C. Understanding real-time time-dependent density-functional theory simulations of ultrafast laser-induced dynamics in organic molecules. *J. Chem. Phys.* **2020**, *153* (5), 054106.
(41) Gelin, M. F.; Huang, X.; Xie, W.; Chen, L.; Došlić, N. a.; Domcke, W. Ab Initio Surface-Hopping Simulation of Femtosecond Transient-Absorption Pump-Probe Signals of Nonadiabatic Excited-State Dynamics Using the Doorway-Window Representation. *J. Chem. Theory Comput.* **2021**, *17* (4), 2394−2408.
(42) Matsika, S. Electronic Structure Methods for the Description of Nonadiabatic Effects and Conical Intersections. *Chem. Rev.* **2021**, *121*, 9407−9449.
(43) Barbatti, M.; Lan, Z.; Crespo-Otero, R.; Szymczak, J. J.; Lischka, H.; Thiel, W. Critical appraisal of excited state nonadiabatic dynamics simulations of 9 H-adenine. *J. Chem. Phys.* **2012**, *137* (22), 22A503.
(44) Tully, J. C. Molecular dynamics with electronic transitions. *J. Chem. Phys.* **1990**, *93* (2), 1061−1071.
(45) Koslowski, A.; Beck, M. E.; Thiel, W. Implementation of a general multireference configuration interaction procedure with analytic gradients in a semiempirical context using the graphical unitary group approach. *J. Comput. Chem.* **2003**, *24* (6), 714−726.
(46) Knowles, P. J.; Werner, H.-J. An efficient second-order MC SCF method for long configuration expansions. *Chem. Phys. Lett.* **1985**, *115* (3), 259−267.
(47) Werner, H. J.; Knowles, P. J. A second order multiconfiguration SCF procedure with optimum convergence. *J. Chem. Phys.* **1985**, *82* (11), 5053−5063.
(48) Shiozaki, T.; Győrffy, W.; Celani, P.; Werner, H.-J. Communication: Extended multi-state complete active space second-order perturbation theory: Energy and nuclear gradients. *J. Chem. Phys.* **2011**, *135* (8), 081106.
(49) Szalay, P. G.; Aquino, A. J.; Barbatti, M.; Lischka, H. Theoretical study of the excitation spectrum of azomethane. *Chem. Phys.* **2011**, *380* (1−3), 9−16.
(50) Gaenko, A.; DeFusco, A.; Varganov, S. A.; Martinez, T. J.; Gordon, M. S. Interfacing the ab initio multiple spawning method with electronic structure methods in GAMESS: Photodecay of trans-azomethane. *J. Phys. Chem. A* **2014**, *118* (46), 10902−10908.
(51) Diau, E. W. G.; Zewail, A. H. Femtochemistry of trans-Azomethane: A Combined Experimental and Theoretical Study. *ChemPhysChem* **2003**, *4* (5), 445−456.
(52) Cattaneo, P.; Persico, M. Semiclassical simulations of azomethane photochemistry in the gas phase and in solution. *J. Am. Chem. Soc.* **2001**, *123* (31), 7638−7645.
(53) Sellner, B.; Ruckenbauer, M.; Stambolic, I.; Barbatti, M.; Aquino, A. J.; Lischka, H. Photodynamics of azomethane: A nonadiabatic surface-hopping study. *J. Phys. Chem. A* **2010**, *114* (33), 8778−8785.
(54) Diau, E. W.-G.; Abou-Zied, O. K.; Scala, A. A.; Zewail, A. H. Femtosecond dynamics of transition states and the concept of concertedness: Nitrogen extrusion of azomethane reactions. *J. Am. Chem. Soc.* **1998**, *120* (13), 3245−3246.
(55) Burton, K. A.; Weisman, R. B. Stepwise photodissociation of vapor-phase azomethane. *J. Am. Chem. Soc.* **1990**, *112* (5), 1804−1807.
(56) Liu, R.; Cui, Q.; Dunn, K. M.; Morokuma, K. Ab initio molecular orbital study of the mechanism of photodissociation of trans-azomethane. *J. Chem. Phys.* **1996**, *105* (6), 2333−2345.
(57) Cattaneo, P.; Persico, M. Diabatic and adiabatic potential-energy surfaces for azomethane photochemistry. *Theor. Chem. Acc.* **2000**, *103* (5), 390−398.
(58) Yan, Y. J.; Mukamel, S. Femtosecond pump-probe spectroscopy of polyatomic molecules in condensed phases. *Phys. Rev. A: At., Mol., Opt. Phys.* **1990**, *41* (11), 6485.
(59) Yan, Y. J.; Fried, L. E.; Mukamel, S. Ultrafast pump-probe spectroscopy: femtosecond dynamics in Liouville space. *J. Phys. Chem.* **1989**, *93* (25), 8149−8162.
(60) Fried, L. E.; Mukamel, S. A classical theory of pump-probe photodissociation for arbitrary pulse durations. *J. Chem. Phys.* **1990**, *93* (5), 3063−3071.
(61) Bosma, W. B.; Yan, Y. J.; Mukamel, S. Intramolecular and solvent dynamics in femtosecond pump-probe spectroscopy. *J. Chem. Phys.* **1990**, *93* (6), 3863−3873.
(62) Hu, D.; Xie, Y.; Peng, J.; Lan, Z. On-the-Fly Symmetrical Quasi-Classical Dynamics with Meyer-Miller Mapping Hamiltonian for the Treatment of Nonadiabatic Dynamics at Conical Intersections. *J. Chem. Theory Comput.* **2021**, *17* (6), 3267−3279.
(63) Hu, D.; Peng, J.; Chen, L.; Gelin, M. F.; Lan, Z. Spectral Fingerprint of Excited-State Energy Transfer in Dendrimers through Polarization-Sensitive Transient-Absorption Pump−Probe Signals: On-the-Fly Nonadiabatic Dynamics Simulations. *J. Phys. Chem. Lett.* **2021**, *12*, 9710−9719.

https://doi.org/10.1021/acs.jpclett.1c03373
J. Phys. Chem. Lett. 2022, 13, 661−668